Reactive and Functional Polymers 191 (2023) 105685

Contents lists available at ScienceDirect

Reactive and Functional Polymers

journal homepage: www.elsevier.com/locate/react

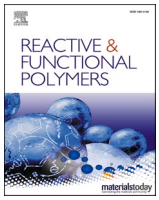

Kraft lignins from different poplar genotypes obtained by selective acid precipitation and their use for the production of electrospun nanostructures

David Ibarra [a,*], Luisa García-Fuentevilla [a], José F. Rubio-Valle [b], Raquel Martín-Sampedro [a], Concepción Valencia [b], María E. Eugenio [a,*]

[a] Instituto de Ciencias Forestales (ICIFOR-INIA), CSIC, Ctra. de la Coruña, km 7,5, 28040 Madrid, Spain
[b] Pro2TecS—Chemical Process and Product Technology Research Centre, Departamento de Ingeniería Química, ETSI, Campus de "El Carmen", Universidad de Huelva, 21071 Huelva, Spain

ARTICLE INFO

Keywords:
Kraft lignins
Electrospinning
Nanostructures
Poplar genotypes
Selective precipitation

ABSTRACT

Kraft lignins from different poplar genotypes (*Populus alba* L. "PO-10-10-20" and *Populus x canadensis* "Ballotino") were isolated by selective acid precipitation (pH 5 and 2.5), chemically and structurally characterized and used together with cellulose acetate (CA) for the manufacture of nanostructures by electrospinning. Generally, lignins showed a predominance of β-β′ resinols substructures (4.7–5.3 linkages per 100 aromatic units) followed by β-O-4′ (1.6–3.3 linkages per 100 aromatic units) and β-5′ phenylcoumarans (0.5–2.4 linkages per 100 aromatic units) and a high abundance of S lignin units (S/G 3.0–4.3). Moreover, lignins showed low molecular weight values (between 5.14 and 5.59 KDa) and high phenolic content (529.1 –644.5 mg GAE/g lignin). Regarding the electrospun nanostructures obtained from Kraft lignins/CA solutions, all of them presented uniform cross-linked nanofibers with a few beaded fibers according to the suitable range values of surface tension (29.18–29.71 mN/cm), electrical conductivity (131.2–158.9 μS/cm) and dynamic viscosity (0.28–0.32 Pa.s) that biopolymer solutions showed. Nevertheless, electrospun Kraft lignins/CA nanostructures with larger mean diameters were generated from lignins at pH 5, which displayed higher phenolic and β-O-4′ contents compared to lignins at pH 2.5. On the other hand, the type of poplar lignin genotype did not exert a significant influence on the mean fiber diameter.

1. Introduction

Fossil fuels-based polymers are widely used to manufacture multitude of essential products that meet today's consumer needs. However, this manufacturing pattern is having a serious impact on global climate change, so there is an urgent need to use natural polymers or biopolymers as an alternative to fossil fuel-based polymers. In this scenario, cellulose, hemicelluloses and lignin, the largest available biopolymers on earth, could play a key role in reversing the traditional fossil fuels-based manufacturing pattern and, consequently in mitigating the severe climate change consequences.

Lignin, together with carbohydrates, is the main cell wall constituent in lignocellulosic biomass. Its complex aromatic and polymeric structure are the result of the oxidative coupling of three typical 4-hydroxyphenylpropanoid units, giving rise to aryl-ether and C—C linkages [1]. Lignin is generated as by-product in a multitude of biorefinery transformation processes that aim to eliminate lignin in order to access potentially valuable carbohydrates. This is the case of the pulp and paper industry, mainly based on Kraft and Sulphite pulping technologies, which generates around 90% of the total lignin produced in the world [2]. Lignin displays different features such as high carbon content (>60 wt%) and hard aromatic structure, among others, which make this lignocellulosic constituent an excelent precursor for high value-added materials and chemicals [3], thereby increasing the sustainability and profitability of pulp and paper industry and promoting the implementation of the circular bioeconomy concept. Among the different valorization approaches, lignin nanofibers manufactured by electrospinning are actually of increasing significance, due to the great potential of these nanostructured materials for numerous engineering applications, such as carbon fiber precursors, supercapacitors, filters, drug delivery and tissue applications [4–7]. The main obstacles to manufacture lignin-based electrospun nanofibers are the great heterogeneity in the chemical composition of lignin, its low molecular weight, its highly random and branched structure and the presence of low molecular weight

* Corresponding author.
E-mail addresses: ibarra.david@inia.csic.es (D. Ibarra), mariaeugenia@inia.csic.es (M.E. Eugenio).

https://doi.org/10.1016/j.reactfunctpolym.2023.105685
Received 21 April 2023; Received in revised form 5 July 2023; Accepted 1 August 2023
Available online 3 August 2023

compounds that are formed by degradation during the delignification process of lignocellulose. Thus, electrospun particles and non-uniform structures formed by particles or globules distributed along the strands in so-called "BOAS" (beads on a string) are frequently obtained [8,9] as a consequence of the lignin chains not becoming sufficiently entangled in the solution [10]. Therefore, lignin-based electrospinning processes usually involve the combination with a second polymer as doping agent, such as polyvinyl acetate, polyethylene oxide, polycaprolactone, polylactic acid and polyvinylpyrrolidone among others, to improve spinnability and generate more uniform nanofibers [11–17]. On the other hand, due to its high electrospinability [18,19], cellulose acetate is a suitable polymeric component to develop lignin-based nanostructures; moreover, cellulose acetate is a biodegradable, renewable, and biocompatible polymer that can be easily obtained from cellulose [20].

Due to the high chemical heterogeneity of lignin generated in pulp and paper processes, it is necessary to fractionate lignin with specific features to be used in a particular application, including the lignin-based nanofibers production by electrospinning. In this respect, there are different methodologies for this purpose, such as the use of selective solvents [21,22], ultrafiltration by membrane technology [23], and fractionation by acid precipitation [24,25]. The latter acid precipitation is the most commonly used technology, decreasing the pH liquor gradually by the addition of mineral acids. This methodology includes acid precipitation to a selective pH, in which all lignin precipitated until reach a specific pH is recovered [24], or sequential acid precipitation, in which pH is modified sequentially from the same single liquor sample, collecting different lignin fractions at different pHs [25].

In the present study, black liquors were obtained by Kraft pulping of different poplar genotypes (*Populus alba* L. "PO-10-10-20" and *Populus x canadensis* "Ballotino"). Poplar (*Populus* spp.) is a fast-growing hardwood species considered for biomass production in different cultivation areas [26], especially in Mediterranean [27], being used as an energy crop as well as for cellulosic pulp production and more newly in the development of novel materials such as nanocellulose [28–30]. Afterthat, the pH of the black liquors was decreased at different levels and the resulting Kraft lignins were characterized by chemical analysis, Fourier transform infrared (FTIR) spectroscopy, ^{13}C and 2D nuclear magnetic resonance, size exclusion chromatography (SEC) and thermal analysis. Subsequently, these poplar Kraft lignins and cellulose acetate were used as base materials for the production of electrospun nanostructures. Thus, the present work aimed to study the physicochemical properties and structural features of lignins from different poplar genotypes recovered by selective precipitation from Kraft black liquors and how they can influence the electrospinning process to produce lignin-based electrospun nanostructures.

2. Materials and methods

2.1. Raw materials and chemicals

Two different poplar genotypes (*Populus alba* L. "PO-10-10-20" and *Populus x canadensis* "Ballotino") were provided by Silviculture and Forest Management Department of ICIFOR-INIA, CSIC (Madrid, Spain). *P. alba* L. "PO-10-10-20" was selected because it is a autochthonous species from Spain (Guadalquivir valley) with high drought and high salinity tolerance [31]. Moreover, this genotype has recently shown moderate rates of wastewater use, showing, among others, high rates of nitrogen attenuation [32]. Regarding "Ballotino", it is an Italian hybrid considered a broadly-adapted genotype to different environmental conditions with an appropiate biomass production [27].

Cellulose acetate (CA) (M_n = 30,000 g/mol, 39.8 wt% acetyl) was provided by Sigma-Aldrich S.A. (Germany) and used as a dopant in the polymeric solution for the electrospinning process. In addition, *N*, *N*-dimethylformamide (DMF) and acetone (Ac), supplied by Sigma Aldrich S.A. (Germany), were employed as solvents to prepare poplar Kraft lignin/CA solutions.

All chemicals were reagent-grade and purchased from Fisher Scientific (Madrid, Spain) or Merck (Madrid, Spain).

2.2. Kraft pulping and lignin recovery

Kraft pulping of poplar genotypes was carried out according to Kang et al. [29]. Afterward, the resulting Kraft pulps (insoluble solids fractions) were filtered, and the black liquors were recovered for selective lignin precipitation (pH lowered to different levels, 5 and 2.5, with concentrated sulphuric acid). The precipitated lignins were denoted as follows: PO-5 and PO-2.5 for Kraft lignins isolated at pH 5 and 2.5, respectively from black liquors of poplar genotype "PO-10-10-20"; and Ba-5 and Ba-2.5 for Kraft lignins isolated at pH 5 and 2.5, respectively from black liquors of poplar genotype "Ballotino".

2.3. Chemical and structural characterization of poplar Kraft lignins

The chemical composition of poplar Kraft lignins was analyzed according to NREL/TP-510-42618 method [33]. Then, after the acid hydrolysis of poplar Kraft lignins, the acid insoluble solid residues (klason lignins) were recovered, whereas the liquid fractions were studied for carbohydrates content by high-performance liquid chromatography (1260 HPLC, Agilent, Waldbronn, Germany, equipped with a G1362A refractive index (RI) detector and an Agilent Hi-Plex H column). Acid-soluble lignins were also determined in the liquid fractions, using a UV–Vis spectrophotometer (Lambda 365, PerkinElmer, Boston, MA, USA) at 205 nm.

The total phenolic content of poplar Kraft lignins was quantified according to Jiménez-López et al. [34] using the Folin-Ciocalteau reagent. Absorbances were measured at 760 nm using the same UV–Vis spectrophotometer described above. A calibration curve prepared from a standard solution of gallic acid was used to quantify the total phenols (expressed as mg gallic acid equivalent (GAE)/g of lignin (on a dry basis)).

Fourier Transform Infrared (FTIR) spectroscopy analysis was performed using a JASCO FT/IR-4200 (Jasco Inc., Japan) spectrophotometer. The spectra were collected in a wavenumber range of 400–4000 cm^{-1}, in the transmission mode, at 4 cm^{-1} resolution [35].

^{13}C NMR experiments were carried out in a Bruker AVANCE 500 MHz (Bruker, USA) spectrometer. Chemical shifts were referred to tetramethylsilane. Deuterated dimethylsulfoxide (DMSO-d_6) was used as a solvent and experiments were recorded according to previous operation conditions [35]. ^{13}C—^{1}H two-dimensional nuclear magnetic resonance (2D NMR) study of Kraft lignins (using DMSO-d_6 as solvent) was recorded in the same spectrometer described above. Heteronuclear Single Quantum Correlation (HSQC) experiment was recorded according to previous operation conditions [35]. Residual DMSO (from DMSO-d_6) was used as an internal reference (δ_C/δ_H 39.6/2.5 ppm). The content of β-O-4′, β-β′ resinol, β-5′ phenylcoumaran, and spirodienones substructures was estimated from C_α–H_α correlations. Cinnamyl alcohol end-groups using C_γ–H_γ correlations, $C_{2,6}$–$H_{2,6}$ correlations from S units; and C_2–H_2 correlations from G units were used to estimate the S/G lignin ratios. $C_{2,6}$–$H_{2,6}$ correlations were used for the estimation of *p*-hydroxybenzoates.

Size exclusion chromatography (SEC) analysis of poplar Kraft lignins was conducted by HPLC (the same equipment described above). Two columns PLgel 10 μm MIXED B 300 × 7.5 mm) connected in series were used. *N*, *N*-dimethylformamide (DMF) was pumped as a mobile phase at the conditions described by Jiménez-López et al. [34]. The calibrations of columns were carried out with polystyrene standards (peak of average molecular weights of 570, 8900, 62,500, 554,000, Sigma-Aldrich, San Luis, MO, USA).

Thermogravimetric analysis (TGA) of poplar Kraft lignins was performed using a thermogravimetric analyser Q-50 (TA Instruments, Newcastle, USA). Mass loss versus temperature curves were determined under N_2 purge. Poplar Kraft lignins were placed on platinum pans and heated from 30 °C to 600 °C, at 10 °C min^{-1} [35].

Differential scanning calorimetry (DSC) measurements of poplar Kraft lignins were conducted with a Q100 calorimeter (TA Instrument Waters, USA) following a heating-cooling-heating program from −50 to 200 °C, at 10 °C min^{-1}. 5–10 mg of poplar Kraft lignin was deposited in hermetically sealed aluminum pans. The sample was purged at a flow rate of 50 mL/min with nitrogen. The glass transition temperature was determined from calorimetric data collected during the second heating ramp.

2.4. Electrospinning

Lignin-based electrospun nanostructures were manufactured based on preliminar studies [36]. For this purpose, solutions of poplar Kraft lignin/CA in DMF/Ac (1:2 v/v) were manufactured at a concentration of 30 wt% using a poplar Kraft lignin: CA weight ratio of 70:30. Then, the solutions were characterized by i) dynamic viscosity in an ARES (Rheometric Scientific, UK) controlled-strain rheometer using a Couette geometry at 25 °C in a shear rate range of 1–300 s^{-1}; ii) electrical conductivity in a CE GP31 high-frequency meter (Crison, Spain); and iii) surface tension using a platinum Wilhelmy plate at room temperature in a Sigma 703D (Biolint Science, Chine) force tensiometer.

Once Kraft lignin/CA solutions were characterized, the nanostructures were generated using DOXA Microfluidics (Malaga, Spain) electrospinning equipment. A horizontal configuration, 15 cm between the aluminum collector plate (cathode) and the tip of the needle (anode), a flow rate of 0.6 mL h^{-1} and a high voltage of 17 kV were used.

The morphology of the electrospun poplar Kraft lignin/CA nanostructures was analyzed using scanning electron microscopy (SEM). For that, a JXA-8200 SuperProbe (JEOL, Japan) was used, being operated at an acceleration voltage of 15 kV, and samples were gold-coated using a sputter coater HHV Scancoat Six SEM [37]. The FIJI ImageJ analysis program was employed to examine the SEM images of the different electrospun nanostructures.

Finally, TGA and DSC analysis of electrospun nanostructures were carried out as previously described for Kraft lignins.

2.5. Statistical analysis

An ANOVA analysis was carried out using at least three replicates of each measure independently. In addition, a means comparison test was performed to detect significant differences ($p < 0.05$).

3. Results and discussion

3.1. Chemical and structural characterization of poplar Kraft lignins

3.1.1. Chemical composition

In general, poplar Kraft lignin samples (PO-5, PO-2.5, Ba-5 and Ba-2.5) presented a high lignin content (total lignin ranging from 91.0% to 98.0%) (Table 1). It can be explained by the chemical structure of poplar native lignin. Its abundance of S units, together with a prevalence of aryl-ether linkages, make poplar native lignin more predisposed to Kraft pulping delignification [38]. The recovered lignin content varied as a function of pH, with yields (g lignin isolated regarding total solids in black liquors) for lignin isolated at pH 5 and 2.5 around 35% and 88%, respectively. García et al. [24] also reported increased lignin precipitation by selective precipitation as the pH of black liquor was decreased. In addition, a high acid-soluble lignin content could be determined in all poplar Kraft lignin samples (5.1–8.7%), being higher for lignins isolated at pH 2.5 than at pH 5 (Table 1). Acid-soluble lignin comprises low-molecular-weight degradation products and hydrophilic derivatives of lignin [39]. Consequently, the amount of low-molecular-weight lignin increased with decreasing precipitation pH, while in parallel, the hydrophilicity of the lignin increased. A similar observation was described by Alekhina et al. [40] when softwood Kraft lignins were isolated sequentially at different pH levels, showing higher acid-soluble lignin amounts in those Kraft lignins precipitated at lower pH values.

Table 1
Chemical composition of poplar Kraft lignins.

	Composition (% dry weight)			
	PO-5	PO-2.5	Ba-5	Ba-2.5
Glucan	1.4	1.3	0.1	0.2
Xylan	2.6	4.1	1.2	2.0
Arabinan	0.2	0.2	0.3	0.3
Acid-soluble Lignin	5.1	6.9	5.3	8.7
Acid-insoluble Lignin	91.0	84.1	92.7	86.9
Total Lignin	96.2	91.0	98.0	95.6

On the other hand, some carbohydrate impurities could be also quantified in all poplar Kraft lignins, ranging from 0.1% to 1.4% for glucan, from 1.2% to 4.1% for xylan, and scarce quantities of arabinan (0.2–0.3%) (Table 1). Carbohydrates solubilized during Kraft pulping, especially hemicelluloses, can partly precipitate due to their low solubility under acidic conditions [40], the reason for which it is observed higher carbohydrate contamination at pH 2.5 compared to pH 5. Nevertheless, the carbohydrate impurities can also be attributed to lignin-carbohydrate complexes [41], which are correlated with the increment of lignin hydrophilicity previously mentioned [39]. These results are similar to those described by Alekhina et al. [40], who suggested that a decrease precipitation pH of softwood Kraft liquor in a sequential way increased the amount of hemicelluloses precipitated together with the lignin.

3.1.2. NMR spectroscopy

2D NMR whole spectra of poplar Kraft lignin samples are presented in Fig. S1; Fig. 1 shows the oxygenated aliphatic region; and Fig. 2 corresponds to the aromatic region. The main $^{13}C—^{1}H$ lignin and carbohydrate correlation signals recognized in spectra are listed in Table 2, assigned according to those described by different published studies [42–49]. The lignin substructures and carbohydrates recognized are displayed in Figs. 3 and 4.

The oxygenated aliphatic region of spectra gave evidence about the different inter-unit linkages present in Kraft lignins (Fig. 1). In spite of the wide β-O-4′ linkage cleavage reported during the Kraft pulping process [50,51], C—H remaining signals from native β-O-4′ substructures (α for G and S lignin units (A_α), β for G units (A_β), and γ (A_γ)) could still be found in all spectra, being more visible in Kraft lignins from genotype “Ballotino” (Figs. 1c and d) compared to lignins from genotype “PO-10-10-20” (Fig. 1a and b). C—H correlation signals from native C—C linkages, such as β-β′ resinols (α (B_α), β (B_β), and the double γ (B_γ)) and β-5′ phenylcoumarans (γ (C_γ)), were also noticiable in all poplar Kraft lignins. Whereas phenylcoumarans are also sensible to degradation during Kraft pulping [48,52], resinols are usually more resistant substructures to alkaline pulping conditions [48,50]. Other C—H correlation signals from native lignin linkages such as spirodienones (α (E_α), and α′ ($E_{\alpha'}$)) and cinnamyl alcohol end-groups (γ (I_γ)) were also found in all Kraft lignin spectra (Fig. 1). Finally, C—H correlation signals from carbohydrates, either from hexose or pentose units, were also visualized in all poplar Kraft lignin spectra (Fig. 1), including signals of xylan chain X_2, X_3, X_4, and X_5, together with the C-1 cross peak for (1–4) β-D-Xylp of xylan (Fig. S1).

Different inter-unit linkages derived during the Kraft pulping process were also identified in the oxygenated aliphatic region (Fig. 1). Among them, C—H correlation signals from epiresinols (α (B'_α), β (B'_β), and γ (B'_γ)) and diaresinol (α (B'_α), β (B'_β), and γ (B'_γ)), both resulting from native resinols [45,49], were detected in all Kraft lignins. In addition, C—H correlation signals of aryl-glycerol (α (AG_α), β (AG_β) and γ (AG_γ)), resulting from non-phenolic β-aryl ether linkage [48], could be tentatively identified in some of the poplar Kraft lignin spectra. Finally, a C—H correlation signal of lignin terminal structures with a carboxyl group in C_β (Ar-CHOH-COOH; α (F_α)), an intermediate in side-chain

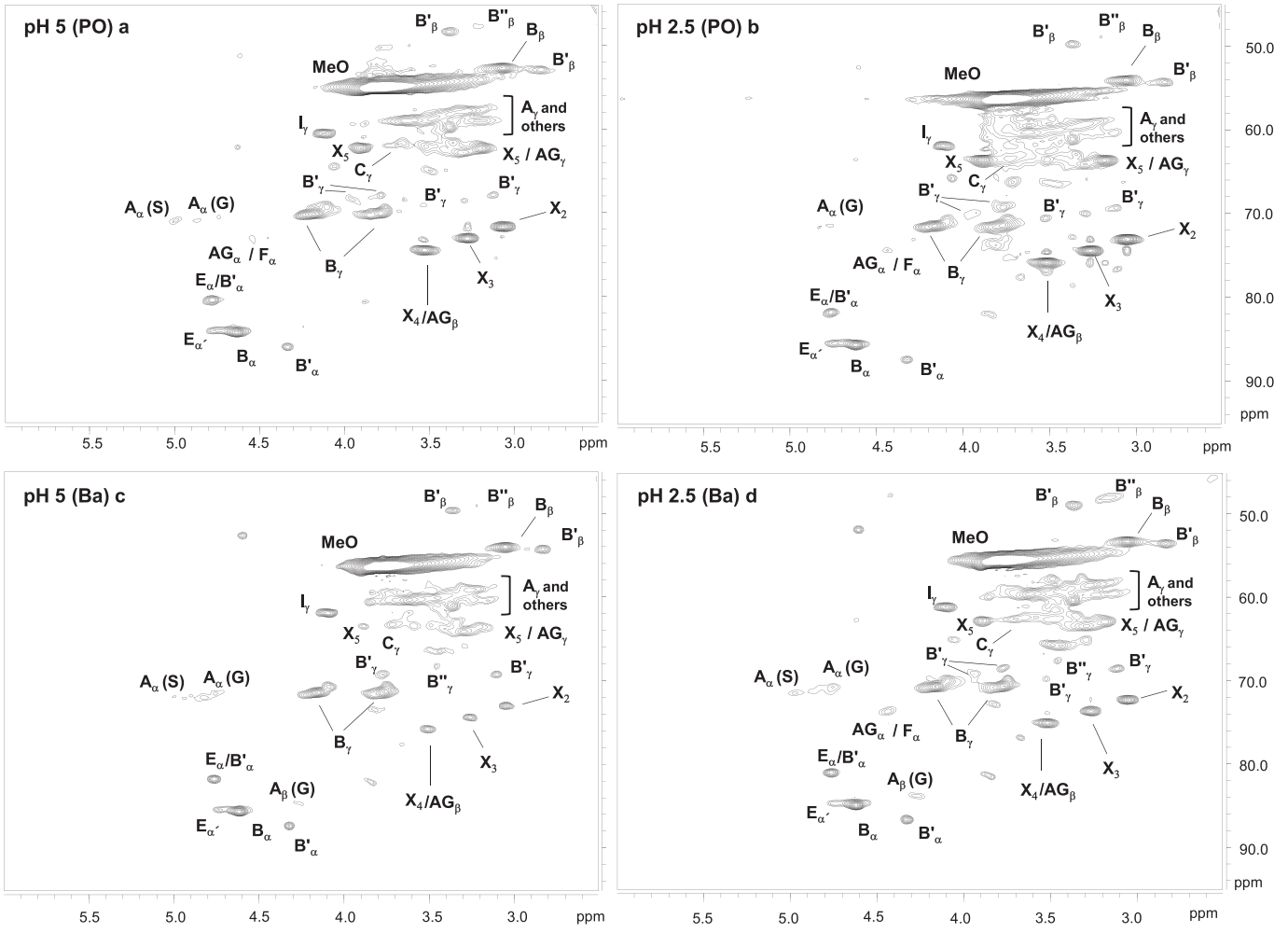

Fig. 1. 2D NMR spectra, δ_C/δ_H 45.0–95.0/2.5–6.0 ppm aliphatic oxygenated region, of PO-5 (a), PO-2.5 (b), Ba-5 (c) and Ba-2.5 (d) Kraft lignins.

degradation [50], could also be observed in some of the poplar Kraft lignin spectra overlapping with the correlation signal of AG_α.

In the aromatic region of poplar Kraft lignins spectra (Fig. 2), the typical C—H correlation signals of S (2,6 ($S_{2,6}$)), G (2 (G_2), 5 (G_5) and 6 (G_6)), and H (2,6 ($H_{2,6}$) and 3,5 ($H_{3,5}$)) lignin units were observed, specific of hardwood lignins [53]. C—H correlation signals for *p*-hydroxybenzoate substructures (2,6 ($PB_{2,6}$) and 3,5 ($PB_{3,5}$)) were also observed in both poplar lignin spectra from genotype "Ballotino".

Signals from Kraft-derived lignin linkages were also identified in the aromatic region of all poplar Kraft lignin spectra. Among them, a group of C—H correlation signals of oxidized lignin units resulting from Kraft pulping [52], with a variety of aldehyde ketone and carboxylic end-groups, could also be detected in all spectra. They included syringaldehyde or acetosyringone ($S'_{2,6}$), vanillin (G'_2 and G'_6), acetovanillone (G'_2 and G'_6), and vanillic acid (G'_6). C—H correlation signals endorsed to β1 stilbene (α ($SB1_\alpha$), from spirodienone degradation, and β5 stilbene (α ($SB5_\alpha$) and β ($SB5_\beta$) respectively), derived from β-5′ phenylcoumaran were also found [42,44]. In the same way, C—H correlation signals attributed to vinyl-ether (α (V_α), from free phenolic β-O-4′ degradation, were also detected, including signals from their two isomers (V_{trans} and V_{cis}) with several combinations of G and S units (V(G–G), V(S–G), V (G—S) and V(S-S)) [49]. Finally, C—H correlation signals for $S_{2,6}$ in $S_{1-1'}$ (3,5-tetramethoxy-para-diphenol), G_2 and G_6 in $G_{1-1'}$ (3-dimethoxy-para-diphenol) and $S_{2,6}$ in S_1-$G_{1'}$ / $G_{5'}$ were also hesitantly recognized, similarly to Kraft lignins from elm, spruce and eucalypt [42–44].

The quantification of inter-unit linkages and cinnamyl end-groups (per 100 aromatic units), the relative abundances of the S, G, and H lignin units (molar percentage), and the *p*-hydroxybenozates, and S/G ratios of the different poplar Kraft lignins are displayed in Table 3. All poplar Kraft lignins exhibited a prevalence of β-β′ resinols substructures (between 4.7 and 5.3 linkages per 100 aromatic units) followed by β-O-4′ substructures (between 1.6 and 3.3 linkages per 100 aromatic units) and β-5′ phenylcoumarans (between 0.5 and 2.4 linkages per 100 aromatic units). These abundances reflect the higher susceptibility of β-O-4′ and phenylcoumarans to degradation under alkaline conditions of Kraft pulping compared to the higher stability showed by β-β′ resinols [50–52]. Consequently, these lignins displayed a high phenolic content, as reflected in ^{13}C NMR and Folin-Ciocalteau analysis. ^{13}C NMR spectra of all poplar Kraft lignins were dominated by phenolic units, with a predominant band in the aromatic region attributed to C_3 and C_5 of phenolic S units (δ_C 147 ppm) compared to non-phenolic units associated with C_3 and C_5 of etherified S units (δ_C 153 ppm) and C_1 of etherified S units (δ_C 135 ppm) (Fig. S2) [54]. Moreover, phenolic content quantified by Folin-Ciocalteau showed a high abundance in all lignins, being slightly higher in lignins isolated at pH 5 (644.5 ± 5.5 mg GAE/g lignin for poplar genotype "PO-10-10-20" and 638.9 ± 9.3 mg GAE/g lignin for poplar genotype "Ballotino") compared to lignins precipitated at pH 2.5 (585.7 ± 12.1 mg GAE/g lignin for poplar genotype "PO-10-10-20" and 529.1 ± 1.0 mg GAE/g lignin for poplar genotype "Ballotino"). Similar behaviour was described by dos Santos et al. [55] when hardwood Kraft lignin was separated by gradient acid precipitation. However, a reverse trend has been described by Alekhina et al. [40] who observed an increase in the phenolic content of softwood Kraft lignin as pH decreased.

Generally, the abundance of native substructures (β-O-4′, β-β′ resinols

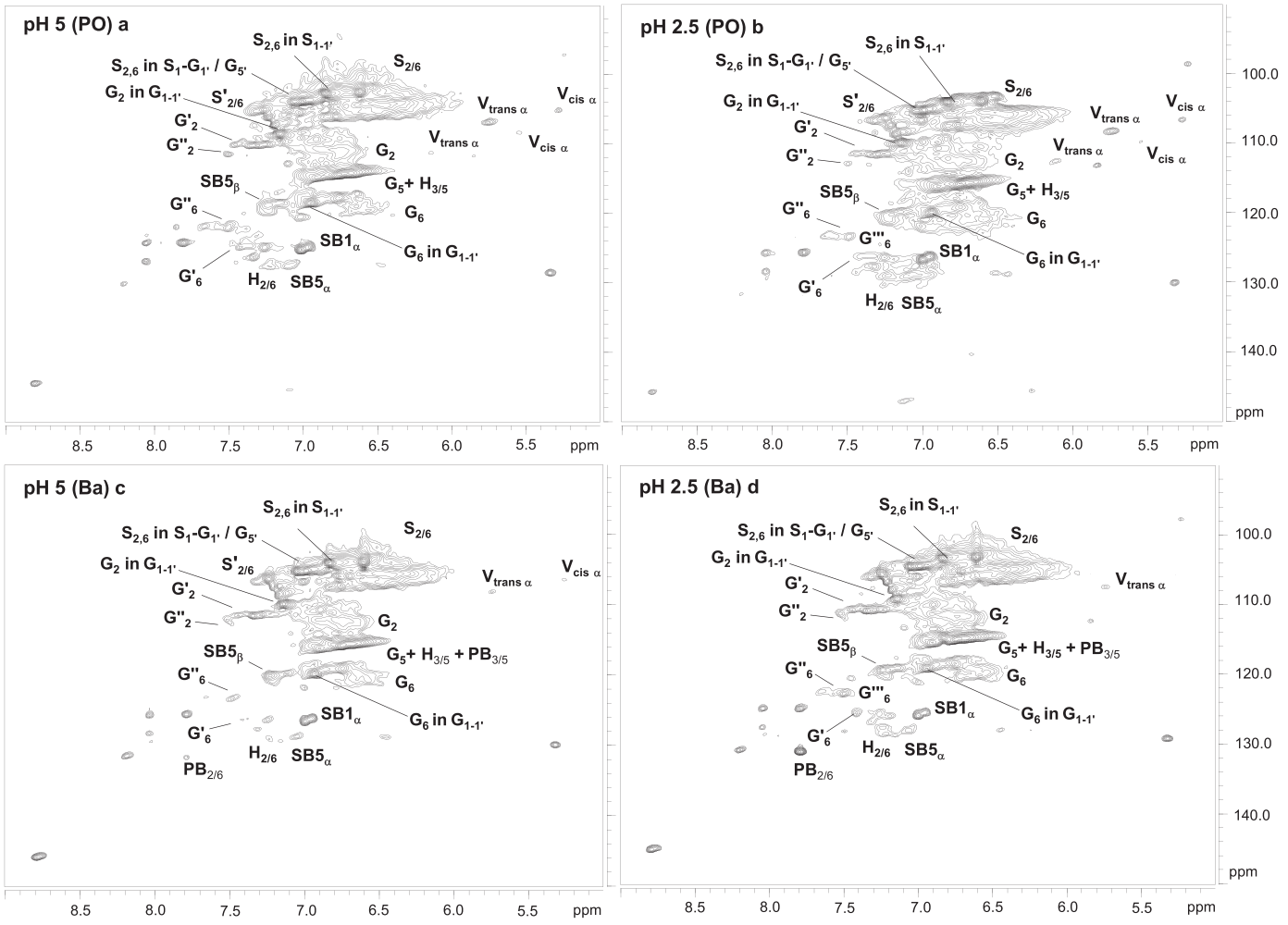

Fig. 2. 2D NMR spectra, δ_C/δ_H 90.0–150.0/5.0–9.0 ppm aromatic region, of PO-5 (a), PO-2.5 (b), Ba-5 (c) and Ba-2.5 (d) Kraft lignins.

and β-5′ phenylcoumarans substructures) was slightly higher in Kraft lignins from poplar genotype "Ballotino", which could suggest a major resistance of this material to alkaline delignification. Moreover, the abundances of β-O-4′ and β-β′ resinols were slightly lower in Kraft lignins from both genotypes isolated at pH 2.5, showing lignin more degraded at lower pH. Contrary, β-5′ phenylcoumarans content increased at pH 2.5, probably caused by lignin repolymerization through condensation [56], which could support the lower phenolic content previously described at this pH. In this sense, Li et al. [57] also observed a decrease in the frequency of β-O-4′ linkages in Kraft lignin as the pH decreased, whereas the frequency of β-β′ resinols and β-5′ phenylcoumarans showed a reverse trend. They explained these effects as follow. In the case of β-O-4′, the hydroxyl group on Cα position of lignin side chain is dehydroxylated after the electrophilic attack of hydrogen cation on Cα, leading to a breakdown of the β-O-4′ ether bond. Regarding the β-5′ condensation, it is initiated by electrophilic attack of hydrogen cation on Cα, forming a Cα cation. Then, β-5′ bond is formed thereafter when C5 of an aromatic ring added onto Cβ through nucleophilic addition. At lower pH (i.e., higher concentration of hydrogen ions) these reactions are favoured. Alekhina et al. [40] also described a rapid reduction in the abundance of aryl-ethers of softwood Kraft lignins with decreasing precipitation pH in a sequential way. However, contrary to that observed herein, Alekhina et al. [40] found a higher content of β-5′ phenylcoumarans at higher pH values.

Aryl-glycerol substructures were also quantified (0.7 linkages per 100 aromatic units for Kraft lignins isolated indistinctly at pH 5–2.5 from genotype "PO-10-10-20"; and 0.8 linkages per 100 aromatic units for Kraft lignin isolated at pH 2.5 from genotype "Ballotino"). Identical abundances were quantified for Ar-CHOH-COOH substructures. Spirodienones substructures showed a slightly higher content in Kraft lignins isolated indistinctly at pH 5–2.5 from genotype "PO-10-10-20" (1.4 linkages per 100 aromatic units) compared to lignins isolated from genotype "Ballotino" (0.9–0.8 linkages per 100 aromatic units) (Table 3). Finally, cinnamyl alcohol end-groups were also quantified, presenting similar abundances (2.7–3.1 linkages per 100 aromatic units) in all Kraft lignins isolated.

Regarding the S/G ratio, all poplar Kraft lignins showed a high abundance of S lignin units (3.0–4.3) (Table 3). It is well-known the preferential solubilization of S lignin units, which are mostly involved in β-O-4′ alkyl-aryl ether in hardwoods [53], during the Kraft pulping process [52]. Higher S/G ratios were observed for lignins isolated at pH 2.5 (4.3 and 3.5 for lignins from genotypes "PO-10-10-20" and "Ballotino", respectively) compared to lignins isolated at pH 5.0 (3.3 and 3.0 for lignins from genotypes "PO-10-10-20" and "Ballotino", respectively). It can be explained by the greater ease of S units to precipitate than G units with increasing proton concentration in an alkaline lignin solution [58]. Under alkaline conditions, solubilized lignin molecules are negatively charged. When the pH is decreased, the hydrogen ions interact with the lignin molecules negatively charged and, consequently the precipitation of lignin occurs. S units has a stronger binding capacity with positive hydrogen under higher acidic conditions compared to G units due to the two electron-donating methoxy groups of S units, which increase the density of the oxygen electron ring of the phenolic hydroxyl.

Table 2
Assignment of main lignin and carbohydrates $^{13}C—^{1}H$ correlation signals in the HSQC spectra of poplar Kraft lignins.

δ_C/δ_H (ppm)	Assignment
48.7/3.16	C_β–H_β, diaresinol substructures (**B″**)
49.7/3.35	C_β–H_β, epiresinol substructures (**B′**)
54.1/2.81	C_β–H_β, epiresinol substructures (**B′**)
53.8/3.07	C_β–H_β, resinol substructures (**B**)
56.2/3.72	C–H, methoxyls (**MeO**)
60.5/3.38–3.65	C_γ–H_γ, β-O-4′ substructures (**A**)
61.8/4.11	C_γ–H_γ, cinnamyl alcohol end groups (**I**)
62.3/3.68	C_γ–H_γ, phenylcoumaran substructures (**C**)
63.3/3.21–3.89	C_5–H_5, xylan
63.6/3.11	C_γ–H_γ, aryl-glycerol (**AG**)
68.2/3.45	C_γ–H_γ, diaresinol substructures (**B″**)
69.4/3.29–3.71	C_γ–H_γ, epiresinol substructures (**B′**)
70.2/3.72–4.10	C_γ–H_γ, epiresinol substructures (**B′**)
71.3/3.77–4.16	C_γ–H_γ, resinol substructures (**B**)
71.7/4.84	C_α–H_α, β-O-4′ **G** unit (**A**)
72.3/4.86	C_α–H_α, β-O-4′**S** unit (**A**)
73.1/3.09	C_2–H_2, xylan
74.0/4.41	C_α–H_α, aryl-glycerol (**AG**)
74.3/3.31	C_3–H_3, xylan
74.2/4.43	C_α–H_α, Ar–CHOH–COOH units (**F**)
75.6/3.48	C_β–H_β, aryl-glycerol (**AG**)
75.9/3.51	C_4–H_4, xylan
81.7/4.76	C_α–H_α, spirodienone substructures (**E**)
81.8/4.76	C_α–H_α, epiresinol substructures (**B′**)
85.6/4.77	C_α –H_α, spirodienone substructures (**E**)
85.5/4.62	C_α–H_α, resinol substructures (**B**)
87.5/4.30	C_α–H_α, epiresinol substructures (**B′**)
101.8/4.31	C-1, (1–4) β-D-Xylp
104.1/6.61	$C_{2,6}$–$H_{2,6}$, S units (**S**)
103.8/6.82	$C_{2,6}$–$H_{2,6}$, 3,5-tetramethoxy-*para*-diphenol substructures (**$S_{1-1'}$**)
105.0/6.9	$C_{2,6}$–$H_{2,6}$, **S_1-$G_{1'}$ / G_5**, substructures
106.5/5.25	C_α–H_α, isomer cis of vinyl ether (**V**) in **S**–**S**
107.1/7.31	$C_{2,6}$–$H_{2,6}$, oxidized (H–C_α = O or H_3C–C_α = O) S units (**S′**)
108.1/5.73	C_α–H_α, isomer trans of vinyl ether (**V**) in **S**–**S**
109.8/5.54	C_α–H_α, isomer cis of vinil ether (**V**) in **S**–**G**
110.1/7.14	C_2–H_2, 3-dimethoxy-*para*-diphenol substructures (**$G_{1-1'}$**)
110.8/6.90	C_2–H_2, G units (**G**)
111.3/7.38	C_2–H_2, oxidized (H–C_α = O) G units (**G′**)
112.5/6.10	C_α–H_α, isomer trans of vinyl ether (**V**) in **S**–**G**
112.9/7.48	C_2–H_2, oxidized (H_3C–C_α = O) G units (**G″**)
114.1/6.6	$C_{3,5}$–$H_{3,5}$, *p*-hydroxybenzoate (**PB**)
115.0/6.73	$C_{3,5}$–$H_{3,5}$, *p*-hydroxyphenyl (**H**)
115.1/6.40–6.79	C_5–H_5, G units (**G**)
119.6/6.77	C_6–H_6, G units (**G**)
119.8/6.95	C_6–H_6, 3-dimethoxy-*para*-diphenol substructures (**$G_{1-1'}$**)
120.3/7.24	C_β–H_β, stilbene (**$SB5_\beta$**)
123.5/7.51	C_6–H_6, oxidized (H_3C–C_α = O) G units (**G″**)
123.7/7.47	C_6–H_6, oxidized (HO–C_α = O) G units (**G‴**)
126.4/6.97	C_α–H_α, stilbene (**$SB1_\alpha$**)
126.7/7.41	C_6–H_6, oxidized (H–C_α = O) G units (**G′**)
128.4/7.14	$C_{2,6}$–$H_{2,6}$, *p*-hydroxyphenyl (**H**)
128.8/7.10	C_α–H_α, stilbene (**$SB5_\alpha$**)
131.6/4.76	$C_{2,6}$–$H_{2,6}$, *p*-hydroxybenzoate (**PB**)

The abundance of stilbene substructures was also quantified in all Kraft lignins, displaying higher quantities in poplar genotype "PO-10-10-20" compared to "Ballotino" (Table 3). In the case of genotype "PO-10-10-20", the abundances were higher for lignins isolated at pH 2.5 (6.7 and 3.5 linkages per 100 aromatic units for stilbene-β1 and stilbene-β5, respectively) compared to those isolated at pH 5 (4.9 and 1.2 linkages per 100 aromatic units for stilbene-β1 and stilbene-β5, respectively). A similar trend was observed for lignins isolated from genotype "Ballotino", showing a higher abundance for stilbene-β1 at pH 2.5 (3.9 linkages per 100 aromatic units) compared to pH 5 (3.1 linkages per 100 aromatic units), and for stilbene-β5 at pH 2.5 (1.5 linkages per 100 aromatic units) compared to pH 5 (1.0 linkages per 100 aromatic units). Vinyl-ether also showed higher quantities in lignins isolated from poplar genotype "PO-10-10-20" (2.5 and 2.3 linkages per 100 aromatic units for lignins isolated at pH 5 and 2.5, respectively) compared to poplar genotype "Ballotino" (0.6 and 0.3 linkages per 100 aromatic units for lignins isolated at pH 5 and 2.5, respectively). Finally, *p*-hydroxybenzoate substructures were also quantified, showing minor amounts for genotype "Ballotino" lignin isolated at pH 5 (0.5) compared to pH 2.5 (2.6).

3.1.3. FTIR spectroscopy

Fig. 5 presents the FTIR spectra of Kraft lignin samples as a function of poplar genotype and pH of selective precipitation. The results show that the FTIR spectra of all poplar kraft lignin samples were very comparable, indicating that there was a similar core structure of the poplar Kraft lignins. The strong and broad band at 3410 cm^{-1} is characteristic of the phenolic and aliphatic OH group's stretching vibration, whereas the typical bands at 1609, 1515, and 1422 cm^{-1} corresponds to aromatic skeleton lignin. As previously commented, the Kraft process tends to mostly degrade the β-O-4′ bonds, yielding a large number of non-etherified phenolic-OH groups in the lignin that were visible in the FTIR spectra at 1362 cm^{-1} [59], as reflected in ^{13}C NMR and Folin-Ciocalteau analysis. Syringyl units in poplar Kraft lignins were observed at 1330 cm^{-1}, while guaiacyl units appeared as a shoulder at 1272 cm^{-1}. Bands at 1150 and 1032 cm^{-1} were characteristic of secondary and primary –OH groups, respectively [60]. The band at 832 cm^{-1} was due to aromatic CH out-of-plane vibration in a p-hydroxyl phenylpropane unit of the syringyl units. Moreover, the band at 1715 cm^{-1} was associated with the carbonyl groups of hemicellulose according to its xylose content or an unconjugated C═O stretching, the latter due to the oxidation of lignin [38], supporting the observations displayed by 2D NMR. All FTIR results obtained were in accordance with those of previous studies [35,61–63].

3.1.4. SEC

The molecular weight distributions of poplar Kraft lignins are displayed in Fig. S3. Weight-average (M_w) and number-average (M_n) molecular weights, as well as molar-mass dispersity (M_w/M_n) values, can be calculated from their molecular weight distributions (Table 4). All poplar Kraft lignins showed low molecular weight values (between 5.14 KDa-5.59 KDa), indicating the high depolymerization of the lignin during the Kraft pulping by the selective breakdown of β-O-4′ alkyl-aryl ether linkages previously showed by 2D NMR (section 3.1.2). Prinsen et al. [52] and Eugenio et al. [42] have already described a significant reduction in the molecular weight values of eucalypt and elm lignins, respectively due to a wild breakdown of β-O-4′ alkyl-aryl ether linkages produced during Kraft pulping process. In general, all poplar Kraft lignins showed similar molecular weight values (Table 4). Kraft lignin from genotype "PO-10-10-20" isolated at pH 5 was slightly higher (5.6 KDa) compared to lignin isolated at pH 2.5 (5.4 KDa). In the same way, Kraft lignin from genotype "Ballotino" isolated at pH 5 was also slightly higher (5.3 KDa) compared to lignin isolated at pH 2.5 (5.1 KDa). On the other hand, similar molar-mass dispersity values were observed for all poplar Kraft lignins (between 1.19 and 1.27). Nevertheless, the chromatogram profiles of the lignins isolated from genotype "PO-10-10-20" were slightly different compared to lignins from genotype "Ballotino", observing two fractions well distinguished: one of them with a lower molecular and the other one with a higher molecular weight. Different studies have shown a clear correlation between molecular weight and sequential acid precipitation. Then, Alekhina et al. [40] described a decrease in molecular weight values of softwood Kraft lignin proportional to the decreasing pH values. Similarly, Lourençon et al. [25] also reported a reduction of molecular weight values of softwood and hardwood Kraft lignins as a function of the pH reduction.

3.1.5. TGA and DSC

The thermal properties of poplar Kraft lignin samples, as a function of genotype and selective acid precipitation, were studied by TGA and DSC. TGA curves, under an inert atmosphere, illustrate the weight loss versus temperature of thermal degradation, while the first derivative of that curve presents the corresponding rate of weight loss. Table 5

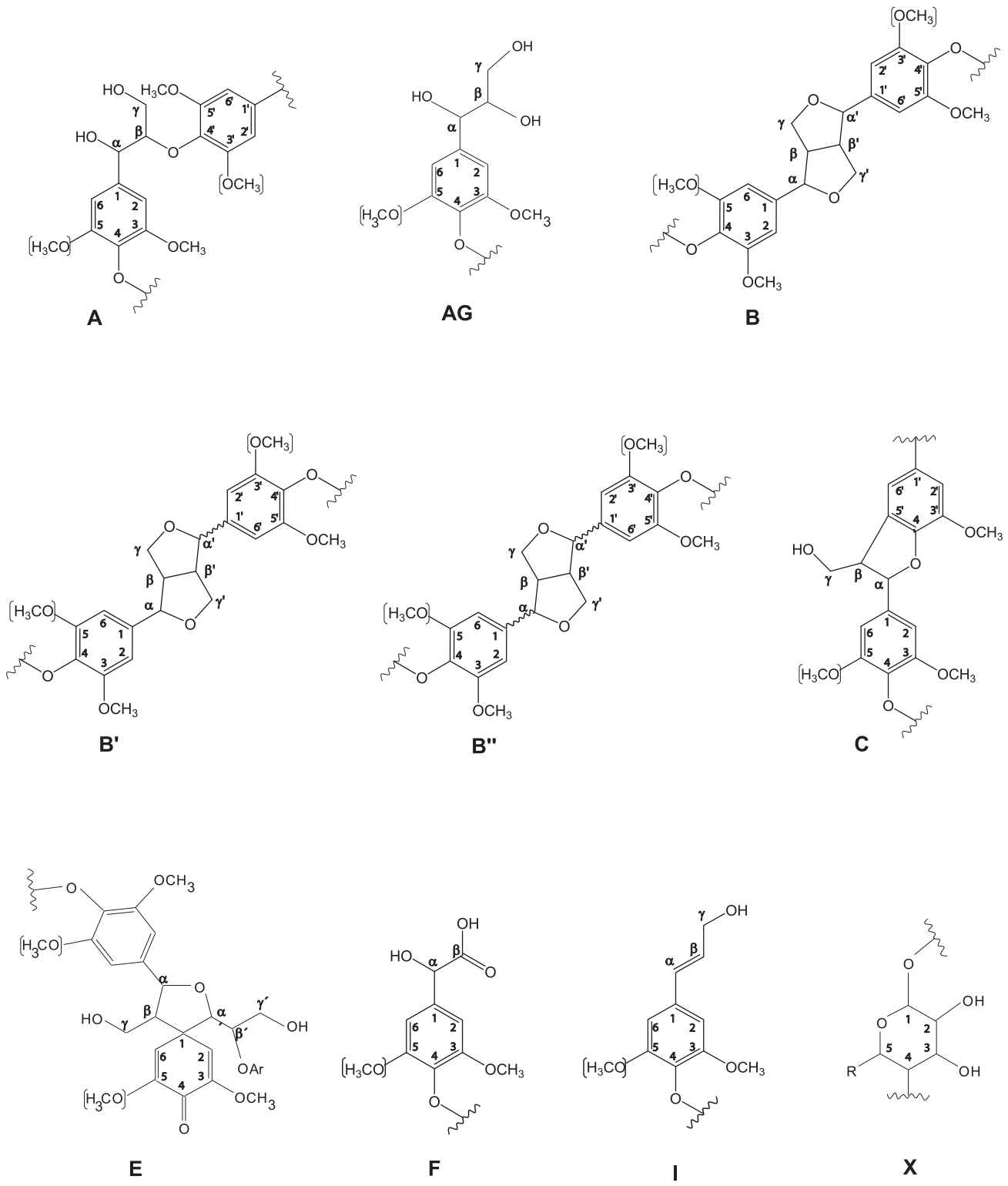

Fig. 3. Lignin and carbohydrate substructures recognized in aliphatic oxygenated region of poplar Kraft lignins: **A**, β-*O*-4′ alkyl-aryl ether; **AG**, aryl-glycerol; **B**, resinols; **B′**, epiresinol; **B″**, diaresinol; **C**, phenylcoumarans; **E**, spirodienones; **F**, Ar–CHOH–COOH; **I**, cinnamyl alcohol end-groups; **X**, xylopyranose (R, OH).

collects the temperature at the beginning of each thermal degradation event (T_{onset}), the temperature related to maximum derivative weight loss (T_{max}), weight loss, and final residue content. In general, all samples showed similar thermal behavior (Fig. 6a and Table 5). All thermograms of lignins were comparable with other studies reported in previous works [63,64]. As can be observed in Fig. 6a, all the lignins exhibited an initial moisture loss of around 3–5%, a weak peak corresponding to hydroxyl dehydration at around 148–160 °C and the main weight loss centered at 333–359 °C with shoulders at 231–271 °C and 424–437 °C, due to several linkages breakdown. The hydroxyl dehydration was not influenced by the poplar genotype, however, a decrease in pH during selective acid precipitation leads to a decrease in the T_{max} of this event. The main weight loss was conditioned by lignin genotype and pH. Thus, poplar Kraft lignins from genotype "PO-10-10-20" show higher thermal

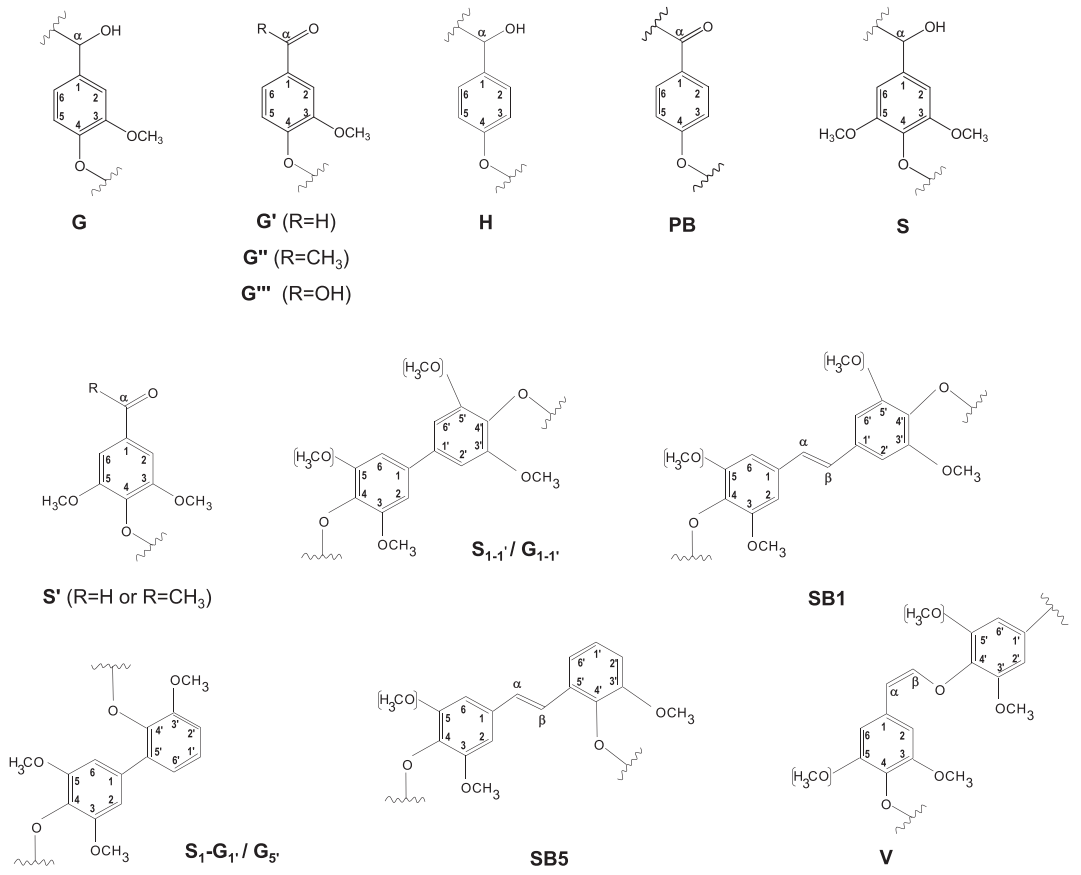

Fig. 4. Lignin substructures recognized in aromatic region of poplar kraft lignins: **G**, guaiacyl unit; **G′**, vanillin; **G′**, acetovanillona; **G′**, vanillic acid; **H**, *p*-hydroxyphenyl unit; **PB**, *p*-benzoate; **S**, syringyl unit; **S′**, syringaldehyde; **S′**, acetosyringone; $\mathbf{S_{1-1'}}$, 3,5-tetramethoxy-*para*-diphenol; $\mathbf{G_{1-1'}}$, 3-dimethoxy-*para*-diphenol; $\mathbf{S_1\text{-}G_1}$, / $\mathbf{G_{5'}}$; **SB1,** stilbene-β-1′; **SB5,** stilbene-β-5′;**V**, vinyl ether.

Table 3
Content of lignin substructures and end-groups (per 100 aromatic units), aromatic units and *p*-hydroxybenzoates (molar percentage) from integration of $^{13}C—^{1}H$ correlation signals in the HSQC spectra of poplar Kraft lignins.

	PO-5	PO-2.5	Ba-5	Ba-2.5
β-O-4′ (**A**)	2.4	1.6	3.3	2.3
Resinols (**B**)	5.0	4.7	5.3	4.9
Phenylcoumarans (**C**)	0.5	2.4	0.8	1.3
Spirodienones (**E**)	1.4	1.4	0.9	0.8
Arylglicerol (**AG**)	0.7	0.7	–	0.8
Ar-CHOH-COOH (**F**)	0.7	0.7	–	0.8
Cinnamyl alcohol end-groups (**I**)	2.9	2.8	3.1	2.7
Stilbene (**SB1**)	4.9	6.7	3.1	3.9
Stilbene (**SB5**)	1.2	3.5	1.0	1.5
Vinyl-ether (**V**)	2.5	2.3	0.6	0.3
H (%)	0.7	0.9	0.3	–
G (%)	22.8	18.6	24.6	23.8
S (%)	76.5	79.5	75.1	75.2
S/G ratio	3.3	4.3	3.0	3.5
p-Benzoate (%)	–	–	0.3	2.6

Content of β-O-4′, resinols, spirodienones, arylglicerol and Ar-CHOH-COOH substructures was estimated by 2D-NMR from C_α–H_α correlations. Cinnamyl alcohol end-groups and phenylcoumarans using C_γ–H_γ correlations; Vinyl-ether and stilbenes (SB1 and SB5) using C_α–H_α correlations; $C_{2,6}$–$H_{2,6}$ correlations from S units; and C_2–H_2 correlations from G units were used to estimate the S/G lignin ratios; $C_{2,6}$–$H_{2,6}$ correlations were used for estimation of *p*-hydroxybenzoates.

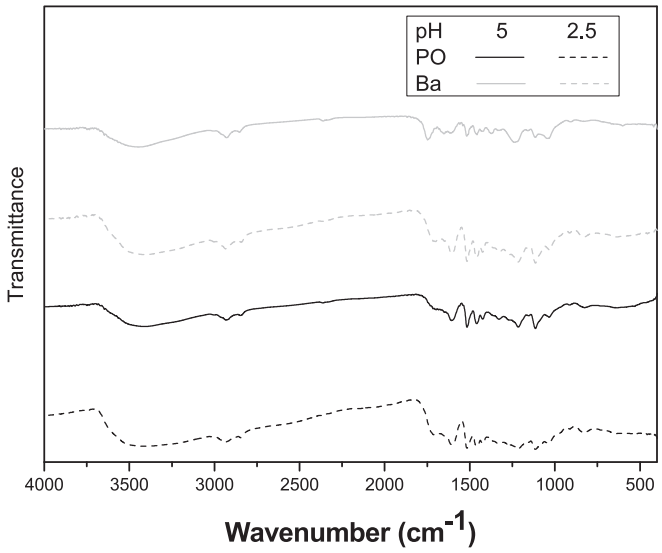

Fig. 5. FTIR spectra of poplar Kraft lignins as a function of genotype and pH of selective acid precipitation.

stability compared to poplar Kraft lignin from "Ballotino". On the other hand, the lower the pH the higher the thermal stability, which can be explained by the higher enrichment of thermostable C—C linkages (especially β-5′) [59] and the lower content of thermally weak β-O-4′ linkages [65,66] observed at lower pH.

The DSC curves and the glass transition temperature (T_g) values of the Kraft lignin samples are exhibited in Fig. 6b and Table 5, respectively. The T_g of lignin is complex to quantify due to the strong electrostatic interactions and because it may depend on several factors, such as molecular weight and the extraction process employed [63]. Nevertheless, the T_g values founds are in good accordance with other works

Table 4
Weight average (M_w) and number-average (M_n) molecular weights and molar-mass dispersity (M_w/M_n) of poplar Kraft lignins. M_w and M_n are given in Da.

	Poplar Kraft lignins			
	PO-5	PO-2.5	Ba-5	Ba-2.5
M_w	5595	5375	5305	5140
M_n	4485	4590	4180	4205
M_w/M_n	1.19	1.21	1.27	1.22

Table 5
TGA characteristics parameters and glass transition temperature of poplar Kraft lignins.

Poplar Kraft lignins	T_{onset} (°C)	T_{max} (°C)	Weight loss (%)	Residue (%)	T_g (°C)
PO-5	164/276	160/237/352/429	1.6/54	40	116
PO-2.5	141/279	151/271/359/437	1.0/50	44	110
Ba-5	170/270	159/231/333/424	1.4/51	44	101
Ba-2.5	148/284	148/231/353/424	1.7/57	38	92

that found T_g values ranging from 90 to 180 °C. [24,59]. Furthermore, the results obtained were associated with their molecular weight values. Thus, T_g values were slightly higher for the poplar Kraft lignins isolated from genotype "PO-10-10-20". On the other hand, poplar Kraft lignins from genotype "PO-10-10-20" and "Ballotino" isolated at pH 5 present T_g values slightly higher compared to poplar Kraft lignin isolated at pH 2.5. According to Methacanon et al. [60], T_g values were the same for lignin precipitated from the black liquor of *Eucalyptus camaldulensis* at pH 2 and 4.

3.2. Characterization of the poplar Kraft lignin/CA solutions

Several authors have reported that the electrospinning process to obtain nanofibers is based on the physicochemical properties of the polymeric solutions [14,67,68]. These properties, such as dynamic viscosity, electrical conductivity and surface tension are displayed in Table 6 for the different poplar Kraft lignin/CA solutions in DMF/Ac as a function of lignin genotype and pH of selective acid precipitation. The dynamic viscosity of the solution can be modified by changing the polymer concentration and the lignin:dopant polymer weight ratio [36]. Thus, there is a specific viscosity level corresponding to the critical concentration of the polymer, which determines semi-diluted unentangled and semi-diluted entangled regimes [69]. Therefore, within the latter, relatively uniform nanofibers are produced. The dynamic viscosity was calculated from viscous flow tests for a concentration of 30 wt % and a poplar Kraft lignin: CA weight ratio of 70:30. All Kraft lignin/CA solutions presented a Newtonian behavior in the range of shear rates studied. In addition, it should be noted that no significant differences were found in the dynamic viscosity values of poplar Kraft lignins with different genotypes nor from the same genotype but precipitated at different pH, with viscosity values between 0.28 and 0.32 Pa.s. As for the electrical conductivity of the solutions, the addition of poplar Kraft lignin/CA leads to a sufficiently good electrical conductivity to the solvent to obtain nanofibers in the electrospinning process [14,36]. The electrical conductivity values displayed by the solutions were within the range of 131.2–158.9 μS/cm. The blend solutions did not present great significant differences between them. Nevertheless, the solutions prepared with PO-2.5 and Ba-2.5 lignins show a slightly higher electrical conductivity, as a consequence of its molecular weight and viscosity, since a lower molecular weight and viscosity leads to higher mobility of ions in the solution [70]. Finally, the surface tension remained around 29.18–29.71 mN/cm for all the poplar kraft lignins studied, showing no significant differences between them and augmenting the surface tension of the DMF/Ac solvent (23.64 mN/cm), which is attributed to improved interactions between the DMF/Ac and lignin/CA. The surface tension values obtained are appropriate to facilitate the electrospinning of lignin solutions with different dopant polymers. Thus, Borrego et al. [14] obtained values in the range of 34–37 mN/cm for low-sulfonate Kraft lignin/polyvinylpyrrolidone solutions in *N,N*-dimethylformamide. On the other hand, Rubio-Valle et al. [36] provided values between 30 and 32.5 mN/cm for solutions of eucalypt Kraft lignin/cellulose acetate at different concentrations and weight ratios of these polymers.

Table 6
Dynamic viscosity, electrical conductivity values and surface tension of poplar Kraft lignin/CA solutions.

	Poplar Kraft lignins/CA			
	PO-5	PO-2.5	Ba-5	Ba-2.5
η (Pa.s)	0.32^{a}	0.29^{a}	0.30^{a}	0.28^{a}
Electrical conductivity (μS/cm)	131.2^{A}	140.8^{A}	137.4^{A}	158.9^{B}
Surface tension (mN/m)	29.55^{α}	29.18^{α}	29.71^{α}	29.33^{α}

Note:Values differing in the superscripts are significantly different ($p < 0.05$).

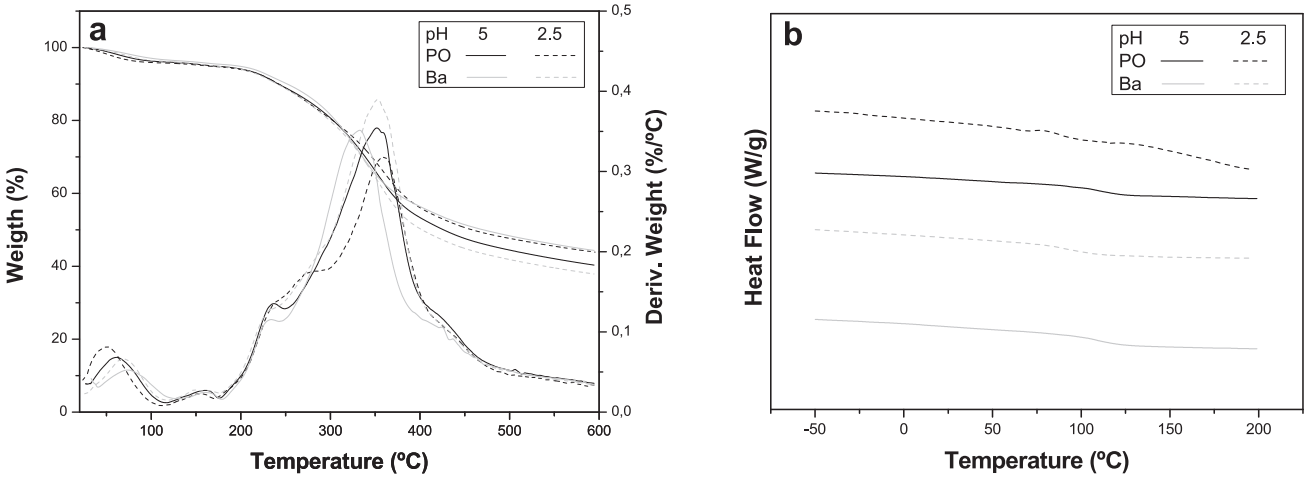

Fig. 6. TGA curves in the form of weight loss and its derived function versus temperature (a) and DSC curves for poplar Kraft lignins (b).

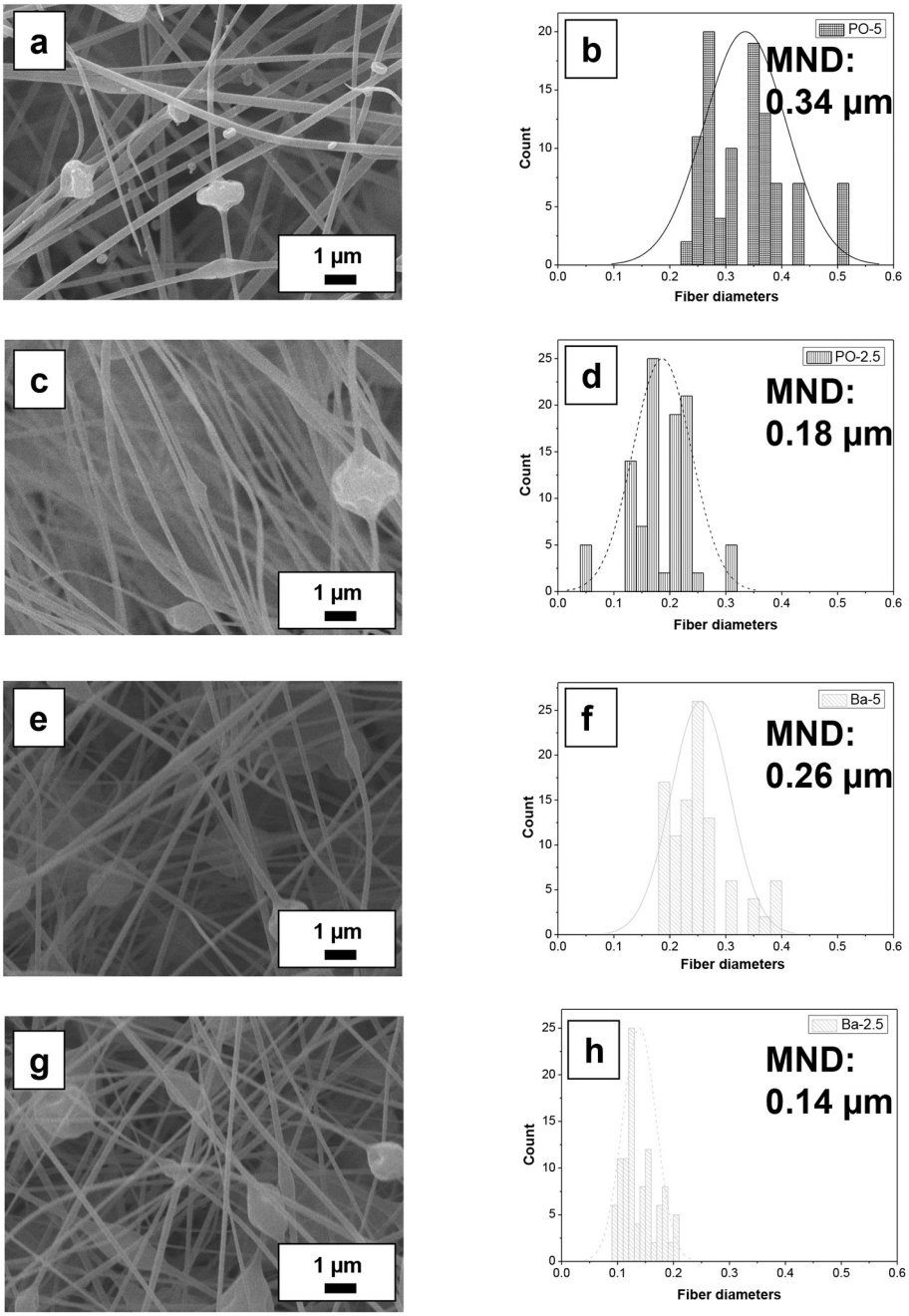

Fig. 7. SEM electrospun nanostructures obtained with different poplar Kraft lignins at x10000 magnification: a) PO-5/CA, c) PO-2.5/CA, e) Ba-5/CA, g) Ba-2.5/CA. Fiber size distribution from SEM electrospun nanostructures for b) PO-5/CA, d) PO-2.5/CA, f) Ba-5/CA, h) Ba-2.5/CA.

3.3. Morphological and thermal properties of electrospun poplar Kraft lignin/CA nanostructures

Fig. 7 shows the micrographs of the electrospun nanostructures obtained by SEM, as well as the fiber distribution, from poplar Kraft lignin/CA solutions at 30 wt% as a function of poplar genotype type and pH of selective acid precipitation. As mentioned above, lignin cannot produce nanofibers given the absence of chain structures and/or molecular entanglements because of its low molecular weight [14,36]. The addition of CA to form blends with lignin improves its electrospinnability and the development of nanofibers, probably as a result of the increase and formation of the entanglements related to the hydrogen bonds between the phenolic and aliphatic hydroxyl groups of the lignins and the acetyl groups of CA [71]. In this sense, the phenolic hydroxyl groups from lignin play a crucial role in these hydrogen networks [72], establishing stronger hydrogen interactions than aliphatic hydroxyl groups. Then, poplar Kraft lignins isolated herein, with high phenolic content (higher in the case of PO-5 and Ba-5 lignins compared to PO-2.5 and Ba-2.5), could thus have good interactions with CA molecules and consequently lead to good spinnability. In this regard, Kubo and Kadla [72] described major hydrogen interactions between phenolic hydroxyl groups of a commercial softwood Kraft lignin and polyethylene oxide (PEO) as doping agent, improving the miscibility of this Kraft lignin. In the same way, Du et al. [73] also reported a better interaction with polyacrylonitrile (PAN) as doping agent with an organosolv lignin from poplar containing higher phenolic hydroxyl content, compared to pine and corn stalk, resulting in enhanced miscibility and spinnability of organosolv poplar lignin. As can be seen, the electrospun nanostructures

obtained from all poplar Kraft lignin/CA solutions present uniform cross-linked nanofibers with a few beaded fibers. Thus, electrospun nanostructures based on PO-5 and PO-2.5 (Fig. 7a and c, respectively) exhibit slightly larger fiber sizes than those obtained at the same pH from Ba-5 and Ba-2.5 (Fig. 7e and g, respectively). On the other hand, it is observed that the electrospun nanostructures obtained from poplar Kraft lignins precipitated at pH 5 present a larger fiber size compared to the ones obtained from those precipitated at pH 2.5. In addition, the fiber diameter distribution (FDD) is also illustrated in Fig. 7 together with the mean fiber size, showing a homogeneous distribution of fibers in the micrograph for all systems. The differences observed in both cases are intrinsically related to the physicochemical properties of the solutions and, more specifically, to the electrical conductivity values. Similarly, García-Fuentevilla et al. [70] described smaller mean nanofiber diameters of nanostructures obtained from olive tree pruning Kraft lignin/CA solution with higher electrical conductivity compared to those manufactured from eucalypt and poplar Kraft lignin/CA solutions with lower electrical conductivity. In addition to this, the morphology of the electrospun poplar Kraft lignin/CA nanostructures was also influenced by the chemical structure of the poplar lignin. It has been reported that lignins with a more linear structure (i.e., higher content of aryl-ether linkages such as β-O-4′ and vinyl-ether substructures, among others) and, therefore less branching (i.e., lower content of carbon-carbon substructures such as resinol, phenylcoumaran an stilbene substructures, among others) display a better spinnability, resulting in nanostructures with higher average diameters [73,74]. It is supported on a better alignment along the doping agent boosting the creation of intermolecular bonds between lignin and the doping agent molecules. Thus, the slightly higher content of β-O-4 and vinyl-ether substructures, observed for both PO-5 and Ba-5 lignin fractions, could improve the alignment along CA, enhancing the interaction between lignin and CA molecules and, consequently the miscibility and spinnability of both lignin fractions as well as the larger average diameters observed for the resulting nanostructures. Contrary, the higher content of carbon-carbon substructures, especially phenylcoumaran and stilbenes, observed for PO-2.5 and Ba-2.5 lignin fractions could explain smaller average diameters displayed for the resulting nanostructures. In this sense, Du et al. [73] described how an organosolv poplar lignin with a structure with higher linearity and less branched, compared to organosolv lignins from pine and corn stalk, was favorable to enhance its spinnability, resulting in nanofibers with the largest average diameters. Zhang et al. [74] observed a better spinnability of a soda lignin enriched in β-O-4 linkages compared to a Kraft lignin containing mostly highly stable β-β' substructures. García-Fuentevilla et al. [70] also studied how the structural characteristics and physicochemical properties of different Kraft lignins, i.e., poplar, olive tree pruning and eucalyptus affected the electrospinning process. In that study, electrospun nanostructures based on crosslinked nanofibers with few bead fibers were associated with higher purity, higher phenolic content, linear structure (correlated with a higher content of β-O-4′ substructures) and higher S/G ratios of lignin samples from poplar and eucalypt compared to olive tree pruning [70]. Therefore, as mentioned above, poplar Kraft lignins isolated at pH 5, compared to poplar Kraft lignins precipitated at pH 2.5, have higher phenolic and aryl-ether bond (β-O-4′) content, as a consequence leading to electrospun poplar Kraft lignin/CA nanostructures with larger mean diameters. On the other hand, the type of poplar Kraft lignin genotype does not exert a significant influence on the mean fiber diameter.

Finally, the thermal properties of electrospun poplar Kraft lignin/CA nanostructures, as a function of genotype and selective acid precipitation, were also evaluated by TGA (Fig. S4) and DSC. In general, all nanostructures presented similar thermal behaviour. As can be seen, thermal stability was slightly higher for electrospun poplar Kraft lignins obtained with lignins precipitated at pH 5. The poplar Kraft lignin genotype at pH 5 did not exert a significant influence on the thermal stability. On the other hand, as it is known, the addition of CA as a dopant increases the glass transition temperatures concerning Kraft lignins [70]. Thus, the glass transition of all electrospun nanostructures was around 129 °C. The genotype and selective acid precipitation do not modify the T_g of electrospun nanostructures.

4. Conclusions

Electrospun lignin/cellulose acetate nanostructures were manufactured using poplar Kraft lignins from different genotypes isolated by selective acid precipitation (pH 5 and 2.5). Poplar Kraft lignins were characterized by their high purity and degradation, showing a scarce content of β-O-4′ alkyl-aryl ether linkages, low molecular weight, and high phenolic content. According to these characteristics, poplar Kraft lignins/cellulose acetate (CA) solutions in dimethylformamide/acetone with suitable properties (surface tension, electrical conductivity and viscosity) for electrospinning were obtained. Then, all electrospun nanostructures showed uniform cross-linked nanofibers with a few beaded fibers. Nevertheless, electrospun poplar Kraft lignin/CA nanostructures manufactured with lignins isolated at pH 5 showed larger mean diameters compared to nanostructures with poplar Kraft lignins precipitated at pH 2.5, which was attributed to the higher phenolic and β-O-4′ contents. On the other hand, the type of poplar lignin genotype did not influence significantly the mean fiber diameter.

CRediT authorship contribution statement

David Ibarra: Conceptualization, Investigation, Writing – original draft, Writing – review & editing, Supervision, Project administration. **Luisa García-Fuentevilla:** Investigation, Writing – review & editing. **José F. Rubio-Valle:** Investigation, Writing – review & editing. **Raquel Martín-Sampedro:** Investigation, Writing – review & editing. **Concepción Valencia:** Conceptualization, Investigation, Writing – original draft, Writing – review & editing, Supervision, Project administration. **María E. Eugenio:** Conceptualization, Investigation, Writing – original draft, Writing – review & editing, Supervision, Project administration.

Declaration of Competing Interest

The authors declare that they have no known competing financial interests or personal relationships that could have appeared to influence the work reported in this paper.

Data availability

Data will be made available on request.

Acknowledgments

This work is part of two coordinated research projects (RTI2018-096080-B-C21 and RTI2018-096080-B-C22) funded by MCIN/AEI/10.13039/501100011033 and by "ERDF A way of making Europe". The authors also wish to thank the Comunidad de Madrid and MCIN/AEI/FEDER, EU for funding this study via Projects SUSTEC-CM S2018/EMT-4348 and TED2021-132122B-C21, respectively. The authors also acknowledge the pre-doctoral grants from José Fernando Rubio Valle (Ref. PRE2019-090632).

Appendix A. Supplementary data

Supplementary data to this article can be found online at https://doi.org/10.1016/j.reactfunctpolym.2023.105685.

References

[1] J. Ralph, K. Lundquist, G. Brunow, F. Lu, H. Kim, P.F. Schatz, J.M. Marita, R. D. Hatfield, S.A. Ralph, J.H. Christensen, W. Boerjan, Lignins: natural polymers from oxidative coupling of 4-hydroxyphenyl- propanoids, Phytochem. Rev. 3 (2004) 29–60, https://doi.org/10.1023/B:PHYT.0000047809.65444.a4.

[2] J.J. Liao, N.H.A. Latif, D. Trache, N. Brosse, M.H. Hussin, Current advancement on the isolation, characterization and application of lignin, Int. J. Biol. Macromol. 162 (2020) 985–1024, https://doi.org/10.1016/j.ijbiomac.2020.06.168.

[3] P. Azadi, O.R. Inderwildi, R. Farnood, D.A. King, Liquid fuels, hydrogen and chemicals from lignin: A critical review, Renew. Sust. Energ. Rev. 21 (2013) 506–523, https://doi.org/10.1016/j.rser.2012.12.022.

[4] M. Kumar, M. Hietala, K. Oksman, Lignin-based electrospun carbon nanofibers, Front. Mater. 6 (2019), https://doi.org/10.3389/fmats.2019.00062.

[5] R. Kumar, A. Butreddy, N. Kommineni, P.G. Reddy, N. Bunekar, C. Sarkar, S. Dutt, V.K. Mishra, K.R. Aadil, Y.K. Mishra, D. Oupicky, A. Kaushik, Lignin: drug/gene delivery and tissue engineering applications, Int. J. Nanomedicine 16 (2021) 2419–2441, https://doi.org/10.2147/IJN.S303462.

[6] P. Schlee, S. Herou, R. Jervis, P.R. Shearing, D.J.L. Brett, D. Baker, O. Hosseinaei, P. Tomani, M.M. Murshed, Y. Li, M.J. Mostazo-López, D. Cazorla-Amorós, A. B. Jorge Sobrido, M.-M. Titirici, Free-standing supercapacitors from Kraft lignin nanofibers with remarkable volumetric energy density, Chem. Sci. 10 (2019) 2980–2988, https://doi.org/10.1039/C8SC04936J.

[7] D. Kim, A. Bahi, L.-Y. Liu, T. Bement, S. Rogak, S. Renneckar, F. Ko, P. Mehrkhodavandi, Poly(Lactide)-modified lignin nanofibers: investigating the role of polymer tacticity on fiber properties and filtration efficiency, ACS Sustain. Chem. Eng. 10 (2022) 2772–2783, https://doi.org/10.1021/acssuschemeng.1c08053.

[8] S. Aslanzadeh, Z. Zhu, Q. Luo, B. Ahvazi, Y. Boluk, C. Ayranci, Electrospinning of colloidal lignin in poly(ethylene oxide) N, N -dimethylformamide solutions, Macromol. Mater. Eng. 301 (2016) 401–413, https://doi.org/10.1002/mame.201500317.

[9] M.S.N. Oliveira, R. Yeh, G.H. McKinley, Iterated stretching, extensional rheology and formation of beads-on-a-string structures in polymer solutions, J. Non-Newtonian Fluid Mech. 137 (2006) 137–148, https://doi.org/10.1016/j.jnnfm.2006.01.014.

[10] I. Dallmeyer, F. Ko, J.F. Kadla, Electrospinning of technical lignins for the production of fibrous networks, J. Wood Chem. Technol. 30 (2010) 315–329, https://doi.org/10.1080/02773813.2010.527782.

[11] M. Ago, K. Okajima, J.E. Jakes, S. Park, O.J. Rojas, Lignin-based electrospun nanofibers reinforced with cellulose nanocrystals, Biomacromolecules. 13 (2012) 918–926, https://doi.org/10.1021/bm201828g.

[12] S. Aslanzadeh, B. Ahvazi, Y. Boluk, C. Ayranci, Morphologies of electrospun fibers of lignin in poly(ethylene oxide)/N,N-dimethylformamide, J. Appl. Polym. Sci. 133 (2016), https://doi.org/10.1002/app.44172.

[13] D. Kai, W. Ren, L. Tian, P.L. Chee, Y. Liu, S. Ramakrishna, X.J. Loh, Engineering poly(lactide)–lignin nanofibers with antioxidant activity for biomedical application, ACS Sustain. Chem. Eng. 4 (2016) 5268–5276, https://doi.org/10.1021/acssuschemeng.6b00478.

[14] M. Borrego, J.E. Martín-Alfonso, M.C. Sánchez, C. Valencia, J.M. Franco, Electrospun lignin-PVP nanofibers and their ability for structuring oil, Int. J. Biol. Macromol. 180 (2021) 212–221, https://doi.org/10.1016/j.ijbiomac.2021.03.069.

[15] D.A. Baker, T.G. Rials, Recent advances in low-cost carbon fiber manufacture from lignin, J. Appl. Polym. Sci. 130 (2013) 713–728, https://doi.org/10.1002/app.39273.

[16] I. Dallmeyer, F. Ko, J.F. Kadla, Correlation of elongational fluid properties to fiber diameter in electrospinning of softwood kraft lignin solutions, Ind. Eng. Chem. Res. 53 (2014) 2697–2705, https://doi.org/10.1021/ie403724y.

[17] E. Stojanovska, E.S. Pampal, A. Kilic, M. Quddus, Z. Candan, Developing and characterization of lignin-based fibrous nanocarbon electrodes for energy storage devices, Compos. Part B 158 (2019) 239–248, https://doi.org/10.1016/j.compositesb.2018.09.072.

[18] R. Konwarh, N. Karak, M. Misra, Electrospun cellulose acetate nanofibers: the present status and gamut of biotechnological applications, Biotechnol. Adv. 31 (2013) 421–437, https://doi.org/10.1016/j.biotechadv.2013.01.002.

[19] H. Liu, Y.-L. Hsieh, Ultrafine fibrous cellulose membranes from electrospinning of cellulose acetate, J. Polym. Sci. B Polym. Phys. 40 (2002) 2119–2129, https://doi.org/10.1002/polb.10261.

[20] P. Sánchez-Cid, J.F. Rubio-Valle, M. Jiménez-Rosado, V. Pérez-Puyana, A. Romero, Effect of solution properties in the development of cellulose derivative nanostructures processed via electrospinning, Polymers. 14 (2022) 665, https://doi.org/10.3390/polym14040665.

[21] J. Domínguez-Robles, T. Tamminen, T. Liitiä, M.S. Peresin, A. Rodríguez, A.-S. Jääskeläinen, Aqueous acetone fractionation of Kraft, organosolv and soda lignins, Int. J. Biol. Macromol. 106 (2018) 979–987, https://doi.org/10.1016/j.ijbiomac.2017.08.102.

[22] H. Li, A.G. McDonald, Fractionation and characterization of industrial lignins, Ind. Crop. Prod. 62 (2014) 67–76, https://doi.org/10.1016/j.indcrop.2014.08.013.

[23] J. Fernández-Rodríguez, X. Erdocia, F. Hernández-Ramos, M.G. Alriols, J. Labidi, Chapter 7 - Lignin separation and fractionation by ultrafiltration, in: M. T. Galanakis (Ed.), C.M.B.T.-S. of F.M. in F. by, Academic Press, 2019, pp. 229–265, https://doi.org/10.1016/B978-0-12-815056-6.00007-3.

[24] A. García, A. Toledano, L. Serrano, I. Egüés, M. González, F. Marín, J. Labidi, Characterization of lignins obtained by selective precipitation, Sep. Purif. Technol. 68 (2009) 193–198, https://doi.org/10.1016/j.seppur.2009.05.001.

[25] T.V. Lourençon, F.A. Hansel, T.A. da Silva, L.P. Ramos, G.I.B. de Muniz, W.L. E. Magalhães, Hardwood and softwood Kraft lignins fractionation by simple sequential acid precipitation, Sep. Purif. Technol. 154 (2015) 82–88, https://doi.org/10.1016/j.seppur.2015.09.015.

[26] R.S. Zalesny, D.M. Donner, D.R. Coyle, W.L. Headlee, An approach for siting poplar energy production systems to increase productivity and associated ecosystem services, For. Ecol. Manag. 284 (2012) 45–58, https://doi.org/10.1016/j.foreco.2012.07.022.

[27] H. Sixto, I. Cañellas, J. van Arendonk, P. Ciria, F. Camps, M. Sánchez, M. Sánchez-González, Growth potential of different species and genotypes for biomass production in short rotation in Mediterranean environments, For. Ecol. Manag. 354 (2015) 291–299, https://doi.org/10.1016/j.foreco.2015.05.038.

[28] C.E. Wyman, B.E. Dale, R.T. Elander, M. Holtzapple, M.R. Ladisch, Y.Y. Lee, C. Mitchinson, J.N. Saddler, Comparative sugar recovery and fermentation data following pretreatment of poplar wood by leading technologies, Biotechnol. Prog. 25 (2009) 333–339, https://doi.org/10.1002/btpr.142.

[29] K.-Y. Kang, B.-M. Jo, J.-S. Oh, S.D. Mansfield, The effects of biopulping on chemical and energy consumption during Kraft pulping of hybrid poplar, Wood Fiber Sci. 35 (2003) 594–600.

[30] D. Ibarra, R. Martín-Sampedro, B. Wicklein, A.M. Borrero-López, C. Valencia, A. Valdehíta, J.M. Navas, M.E. Eugenio, L. Populusalba, An autochthonous species of Spain: A source for cellulose nanofibers by chemical pretreatment, Polymers. 14 (2022), https://doi.org/10.3390/polym14010068.

[31] H. Sixto, B.D. González-González, J.J. Molina-Rueda, A. Garrido-Aranda, M. M. Sanchez, G. López, F. Gallardo, I. Cañellas, F. Mounet, J. Grima-Pettenati, F. Cantón, et al., *Eucalyptus* spp. and *Populus* spp. coping with salinity stress: an approach on growth, physiological and molecular features in the context of short rotation coppice (SRC), Trees 30 (2016) 1873–1891, https://doi.org/10.1007/s00468-016-1420-7.

[32] R. Pradana, I. González, N. Oliveira, B.D. González-González, I. de Bustamante, H. Sixto. Suitability of Salicaceae Genotypes to Produce Biomass using Industrial Wastewater. Available at SSRN: https://ssrn.com/abstract=4335380 or 10.2139/ssrn.4335380.

[33] NREL, TP-510-42618 - determination of structural carbohydrates and lignin in biomass, Chem. Anal. Test. Lab. Anal. Proced. Natl. Renew. Energy Lab. (2011).

[34] L. Jiménez-López, R. Martín-Sampedro, M.E. Eugenio, J.I. Santos, H. Sixto, I. Cañellas, D. Ibarra, Co-production of soluble sugars and lignin from short rotation white poplar and black locust crops, Wood Sci. Technol. 54 (2020) 1617–1643, https://doi.org/10.1007/s00226-020-01217-x.

[35] A.M. Borrero-López, R. Martín-Sampedro, D. Ibarra, C. Valencia, M.E. Eugenio, J. M. Franco, Evaluation of lignin-enriched side-streams from different biomass conversion processes as thickeners in bio-lubricant formulations, Int. J. Biol. Macromol. 162 (2020) 1398–1413, https://doi.org/10.1016/j.ijbiomac.2020.07.292.

[36] J.F. Rubio-Valle, M.C. Sánchez, C. Valencia, J.E. Martín-Alfonso, J.M. Franco, Production of lignin/cellulose acetate fiber-bead structures by electrospinning and exploration of their potential as green structuring agents for vegetable lubricating oils, Ind. Crop. Prod. 188 (2022), 115579, https://doi.org/10.1016/j.indcrop.2022.115579.

[37] R. Erdem, M. İlhan, E. Sancak, Analysis of EMSE and mechanical properties of sputter coated electrospun nanofibers, Appl. Surf. Sci. 380 (2016) 326–330, https://doi.org/10.1016/j.apsusc.2015.11.204.

[38] T.-Q. Yuan, S.-N. Sun, F. Xu, R.-C. Sun, Structural characterization of lignin from triploid of Populus tomentosa Carr, J. Agric. Food Chem. 59 (2011) 6605–6615, https://doi.org/10.1021/jf2003865.

[39] S. Yasuda, K. Fukushima, A. Kakehi, Formation and chemical structures of acid-soluble lignin I: sulfuric acid treatment time and acid-soluble lignin content of hardwood, J. Wood Sci. 47 (2001) 69–72, https://doi.org/10.1007/BF00776648.

[40] M. Alekhina, O. Ershova, A. Ebert, S. Heikkinen, H. Sixta, Softwood Kraft lignin for value-added applications: fractionation and structural characterization, Ind. Crop. Prod. 66 (2015) 220–228, https://doi.org/10.1016/j.indcrop.2014.12.021.

[41] M. Lawoko, G. Henriksson, G. Gellerstedt, Characterisation of lignin-carbohydrate complexes (LCCs) of spruce wood (Picea abies L.) isolated with two methods, Holzforschung. 60 (2006) 156–161, https://doi.org/10.1515/HF.2006.025.

[42] M.E. Eugenio, R. Martín-Sampedro, J.I. Santos, B. Wicklein, J.A. Martín, D. Ibarra, Properties versus application requirements of solubilized lignins from an elm clone during different pre-treatments, Int. J. Biol. Macromol. 181 (2021) 99–111, https://doi.org/10.1016/j.ijbiomac.2021.03.093.

[43] N. Giummarella, I.V. Pylypchuk, O. Sevastyanova, M. Lawoko, New structures in eucalyptus Kraft lignin with complex mechanistic implications, ACS Sustain. Chem. Eng. (2020), https://doi.org/10.1021/acssuschemeng.0c03776 acssuschemeng.0c03776.

[44] N. Giummarella, P.A. Lindén, D. Areskogh, M. Lawoko, Fractional profiling of Kraft lignin structure: unravelling insights on lignin reaction mechanisms, ACS Sustain. Chem. Eng. 8 (2020) 1112–1120, https://doi.org/10.1021/acssuschemeng.9b06027.

[45] C.S. Lancefield, H.L.J. Wienk, R. Boelens, B.M. Weckhuysen, P.C.A. Bruijnincx, Identification of a diagnostic structural motif reveals a new reaction intermediate and condensation pathway in Kraft lignin formation, Chem. Sci. 9 (2018) 6348–6360, https://doi.org/10.1039/C8SC02000K.

[46] R. Martín-Sampedro, J.I. Santos, Ú. Fillat, B. Wicklein, M.E. Eugenio, D. Ibarra, Characterization of lignins from Populus alba L. generated as by-products in different transformation processes: Kraft pulping, organosolv and acid hydrolysis, Int. J. Biol. Macromol. 126 (2019), https://doi.org/10.1016/j.ijbiomac.2018.12.158.

[47] L. Ralph, S.A. Ralph, J. Landucci, Database of Lignin and Cell Wall Model Compounds, US Forest Products Laboratory, Madison, WI 2006, 2006 (Available at Services/docs.htm?docids10491, access).

[48] C. Zhao, J. Huang, L. Yang, F. Yue, F. Lu, Revealing structural differences between alkaline and Kraft Lignins by HSQC NMR, Ind. Eng. Chem. Res. 58 (2019) 5707–5714, https://doi.org/10.1021/acs.iecr.9b00499.

[49] C. Zhao, Z. Hu, L. Shi, C. Wang, F. Yue, S. Li, H. Zhang, F. Lu, Profiling of the formation of lignin-derived monomers and dimers from Eucalyptus alkali lignin, Green Chem. 22 (2020) 7366–7375, https://doi.org/10.1039/D0GC01658F.
[50] D. Ibarra, M.I. Chávez, J. Rencoret, J.C. Del Río, A. Gutiérrez, J. Romero, S. Camarero, M.J. Martínez, J. Jiménez-Barbero, A.T. Martínez, Lignin modification during Eucalyptus globulus Kraft pulping followed by totally chlorine-free bleaching: A two-dimensional nuclear magnetic resonance, Fourier transform infrared, and pyrolysis−gas chromatography/mass spectrometry study, J. Agric. Food Chem. 55 (2007) 3477–3490, https://doi.org/10.1021/jf063728t.
[51] C. Fernández-Costas, S. Gouveia, M.A. Sanromán, D. Moldes, Structural characterization of Kraft lignins from different spent cooking liquors by 1D and 2D nuclear magnetic resonance spectroscopy, Biomass Bioenergy 63 (2014) 156–166, https://doi.org/10.1016/j.biombioe.2014.02.020.
[52] P. Prinsen, J. Rencoret, A. Gutiérrez, T. Liitiä, T. Tamminen, J.L. Colodette, M.Á. Berbis, J. Jiménez-Barbero, Á.T. Martínez, J.C. del Río, Modification of the lignin structure during alkaline delignification of eucalyptus wood by Kraft, soda-AQ, and soda-O 2 cooking, Ind. Eng. Chem. Res. 52 (2013) 15702–15712, https://doi.org/10.1021/ie401364d.
[53] J. Rencoret, G. Marques, A. Gutiérrez, D. Ibarra, J. Li, G. Gellerstedt, J.I. Santos, J. Jiménez-Barbero, Á.T. Martínez, J.C. del Río, Structural characterization of milled wood lignins from different eucalypt species, Holzforschung. 62 (2008), https://doi.org/10.1515/HF.2008.096.
[54] H. Wang, Z. Liu, L. Hui, L. Ma, X. Zheng, J. Li, Y. Zhang, Understanding the structural changes of lignin in poplar following steam explosion pretreatment, Holzforschung. 74 (2020) 275–285, https://doi.org/10.1515/hf-2019-0087.
[55] P.S.B. dos Santos, X. Erdocia, D.A. Gatto, J. Labidi, Characterization of Kraft lignin separated by gradient acid precipitation, Ind. Crop. Prod. 55 (2014) 149–154, https://doi.org/10.1016/j.indcrop.2014.01.023.
[56] Q. Sun, Y. Pu, X. Meng, T. Wells, A.J. Ragauskas, Structural transformation of isolated poplar and switchgrass Lignins during dilute acid treatment, ACS Sustain. Chem. Eng. 3 (2015) 2203–2210, https://doi.org/10.1021/acssuschemeng.5b00426.
[57] Q. Li, M.T. Naik, H.-S. Lin, C. Hu, W.K. Serem, L. Liu, P. Karki, F. Zhou, J.S. Yuan, Tuning hydroxyl groups for quality carbon fiber of lignin, Carbon. 139 (2018) 500–511, https://doi.org/10.1016/j.carbon.2018.07.015.
[58] L. Zhang, W. Peng, F. Wang, H. Bao, P. Zhan, J. Chen, Z. Tong, Fractionation and quantitative structural analysis of lignin from a lignocellulosic biorefinery process by gradient acid precipitation, Fuel. 309 (2022), 122153, https://doi.org/10.1016/j.fuel.2021.122153.
[59] A. Tejado, C. Peña, J. Labidi, J.M. Echeverria, I. Mondragon, Physico-chemical characterization of lignins from different sources for use in phenol–formaldehyde resin synthesis, Bioresour. Technol. 98 (2007) 1655–1663, https://doi.org/10.1016/j.biortech.2006.05.042.
[60] P. Methacanon, U. Weerawatsophon, M. Thainthongdee, P. Lekpittaya, Optimum conditions for selective separation of Kraft lignin, Nat. Sci. 44 (2010) 680–690.
[61] A. Martínez, G. Almendros, F. González-Vila, R. Fründ, Solid-state spectroscopic analysis of lignins from several austral hardwoods, Solid State Nucl. Magn. Reson. 15 (1999) 41–48, https://doi.org/10.1016/S0926-2040(99)00045-4.
[62] J.I. Santos, R. Martín-Sampedro, Ú. Fillat, J.M. Oliva, M.J. Negro, M. Ballesteros, M.E. Eugenio, D. Ibarra, Evaluating lignin-rich residues from biochemical ethanol production of wheat straw and olive tree pruning by FTIR and 2D-NMR, Int. J. Polym. Sci. 2015 (2015) 1–11, https://doi.org/10.1155/2015/314891.
[63] M. Fodil Cherif, D. Trache, N. Brosse, F. Benaliouche, A.F., Tarchoun, comparison of the physicochemical properties and thermal stability of organosolv and Kraft lignins from hardwood and softwood biomass for their potential valorization, Waste Biomass Valoriz. 11 (2020) 6541–6553, https://doi.org/10.1007/s12649-020-00955-0.
[64] M. El Moustaqim, A. El Kaihal, M. El Marouani, S. Men-La-Yakhaf, M. Taibi, S. Sebbahi, S. El Hajjaji, F. Kifani-Sahban, Thermal and thermomechanical analyses of lignin, Sustain. Chem. Pharm. 9 (2018) 63–68, https://doi.org/10.1016/j.scp.2018.06.002.
[65] Y. Guo, J. Zhou, J. Wen, G. Sun, Y. Sun, Structural transformation of triploid of Populus tomentosa Carr. Lignin during auto-catalyzed etanol organosolv pretreatment, Ind. Crop. Prod. 76 (2015) 522–529, https://doi.org/10.1016/j.indcrop.2015.06.020.
[66] A. Toledano, L. Serrano, A. Garcia, I. Mondragon, J. Labidi, Comparative study of lignin fractionation by ultrafiltration and selective precipitation, Chem. Eng. J. 157 (2010) 93–99, https://doi.org/10.1016/j.cej.2009.10.056.
[67] J.F. Rubio-Valle, M. Jiménez-Rosado, V. Perez-Puyana, A. Guerrero, A. Romero, Electrospun nanofibres with antimicrobial activities, in: Antimicrobial Textiles from Natural Resources, Elsevier, 2021, pp. 589–618, https://doi.org/10.1016/B978-0-12-821485-5.00020-2.
[68] M. Borrego, J.E. Martín-Alfonso, C. Valencia, M.C. Sánchez, J.M. Franco, Influence of surfactants on the electrospinnability of lignin-PVP solutions and subsequent oil structuring properties of nanofiber mats, Polym. Bull. (2022), https://doi.org/10.1007/s00289-022-04382-0.
[69] J.F. Rubio-Valle, M.C. Sánchez, C. Valencia, J.E. Martín-Alfonso, J.M. Franco, Electrohydrodynamic processing of PVP-doped Kraft lignin micro- and nano-structures and application of electrospun nanofiber templates to produce Oleogels, Polymers. 13 (2021) 2206, https://doi.org/10.3390/polym13132206.
[70] L. García-Fuentevilla, J.F. Rubio-Valle, R. Martín-Sampedro, C. Valencia, M. E. Eugenio, D. Ibarra, Different Kraft lignin sources for electrospun nanostructures production: influence of chemical structure and composition, Int. J. Biol. Macromol. 214 (2022) 554–567, https://doi.org/10.1016/j.ijbiomac.2022.06.121.
[71] M. Schreiber, S. Vivekanandhan, A.K. Mohanty, M. Misra, Iodine treatment of lignin–cellulose acetate electrospun fibers: enhancement of green fiber carbonization, ACS Sustain. Chem. Eng. 3 (2015) 33–41, https://doi.org/10.1021/sc500481k.
[72] S. Kubo, J.F. Kadla, Hydrogen bonding in lignin: a fourier transform infrared model compound study, Biomacromolecules 6 (2005) 2815–2821, https://doi.org/10.1021/bm050288q.
[73] B. Du, H. Zhu, L. Chai, J. Cheng, X. Wang, X. Chen, J. Zhou, R.-C. Sun, Effect of lignin structure in different biomass resources on the performance of lignin-based carbon nanofibers as supercapacitor electrode, Ind. Crop. Prod. 170 (2021), 113745, https://doi.org/10.1016/j.indcrop.2021.113745.
[74] R. Zhang, Q. Du, L. Wang, Z. Zheng, L. Guo, X. Zhang, X. Yang, H. Yu, Unlocking the response of lignin structure for improved carbon fiber production and mechanical strength, Green Chem. 21 (2019) 4981–4987, https://doi.org/10.1039/C9GC01632E.